Journal of Structural Geology 30 (2008) 1317–1331

Contents lists available at ScienceDirect

Journal of Structural Geology

journal homepage: www.elsevier.com/locate/jsg

Slipped deformation bands: A new type of cataclastic deformation bands in Western Sinai, Suez rift, Egypt

Atle Rotevatn [a,b,*,1], Anita Torabi [a,b], Haakon Fossen [a,b], Alvar Braathen [a,2]

[a] Centre for Integrated Petroleum Research, University of Bergen, Box 7800, 5020 Bergen, Norway
[b] Department of Earth Science, University of Bergen, Box 7800, 5020 Bergen, Norway

ARTICLE INFO

Article history:
Received 21 August 2007
Received in revised form 8 June 2008
Accepted 27 June 2008
Available online 6 August 2008

Keywords:
Deformation bands
Cataclasis
Fault
Porous sandstone

ABSTRACT

A type of cataclastic deformation band that features a central discrete slip surface within separate, individual bands is described. Slip surface development is normally constrained to the eventual brittle failure of a deformation band cluster zone due to strain hardening and sequential growth of deformation bands. The deformation bands described herein deviate from this model and, in comparison with classical cataclastic deformation bands previously described in the literature, feature more intense cataclasis, higher offsets, lower permeability but higher porosity. We present evidence suggesting that the bands of this study strain soften during their evolution. Thus, they can accumulate higher strains than classical cataclastic bands and are prone to be reactivated during progressive deformation. The bands appear to have formed under simple shear with minor compaction, following an evolution of (1) band nucleation by grain fracturing and crushing, (2) progressive cataclasis, (3) nucleation of a central fracture, and (4) slippage along the fracture – the end result is referred to as a 'slipped deformation band'. Widespread background, intragranular fracturing of the host rock and relatively high porosity in the bands are suggested as the most probable causes of deviation from traditional models for tectonic deformation in high porosity sandstones.

1. Introduction

A fundamental understanding of faulting in porous media is essential for structural geologists working with the deformation of sedimentary rocks. The topic has been the subject of keen interest, partly due to its relevance in water and, particularly, hydrocarbon reservoirs (e.g. Antonellini and Aydin, 1995; Hesthammer and Fossen, 2001; Shipton et al., 2002). Faulted siliciclastic rocks require some special considerations, as fault initiation and deformation mechanisms in highly porous rocks differ from those in low or non-porous rocks. Of particular interest is the fact that the pore space within the rock volume facilitates some characteristic deformation processes. These include: (1) rigid grain reorganization (granular flow) resulting in compaction, dilation or isochoric strain; (2) grain fracturing/crushing (cataclasis) related to high stress concentrations at grain contact points (e.g. Antonellini et al., 1994). The resulting structural elements are generally referred to as *deformation bands* (Aydin, 1978, also known as shear bands, granulation seams and microfaults) – tabular–planar deformation structures along which shear takes place.

Deformation bands differ from discrete fault surfaces in a number of ways. Primarily, they do not exhibit a discrete and continuous slip plane (grain-scale microfractures do, however, exist), but rather a shear zone of less than a few millimetres width, across which displacement is distributed. They feature offsets on a mm- to cm-scale, and lengths ranging from less than one to tens of metres. Single deformation bands longer than 100 m are rare. The displacement–length ratio of (cataclastic) deformation bands is generally found to be significantly lower than that of faults (Fossen and Hesthammer, 1997; Wibberley et al., 2000).

Classified by deformation mechanism (following Fossen et al., 2007), there are two main types of deformation bands. One is known as *disaggregation bands* (e.g. Mandl et al., 1977; Bense et al., 2003); a sub-type of these is known as *phyllosilicate bands* (framework phyllosilicate bands of Knipe et al., 1997). Disaggregation bands form by localized grain reorganization, but practically no grain crushing. This type of band is the most common type of band at shallow deformation depths. The other type is referred to as *cataclastic bands* (e.g. Aydin, 1978; Aydin and Johnson, 1983; Davis, 1999), as grain crushing or cataclasis is an important mechanism. Cataclastic bands are favoured by high confining pressures (e.g.

* Corresponding author. Department of Earth Science, University of Bergen, Box 7800, 5020 Bergen, Norway. Tel.: +47 481 09 959; fax: +47 553 68 798.
E-mail address: atle.rotevatn@rocksource.com (A. Rotevatn).
[1] Present address: Rocksource ASA, Box 994 Sentrum, 5808 Bergen, Norway.
[2] Present address: The University Centre in Svalbard, Box 156, 9171 Longyearbyen, Norway.

0191-8141/$ – see front matter © 2008 Elsevier Ltd. All rights reserved.
doi:10.1016/j.jsg.2008.06.010

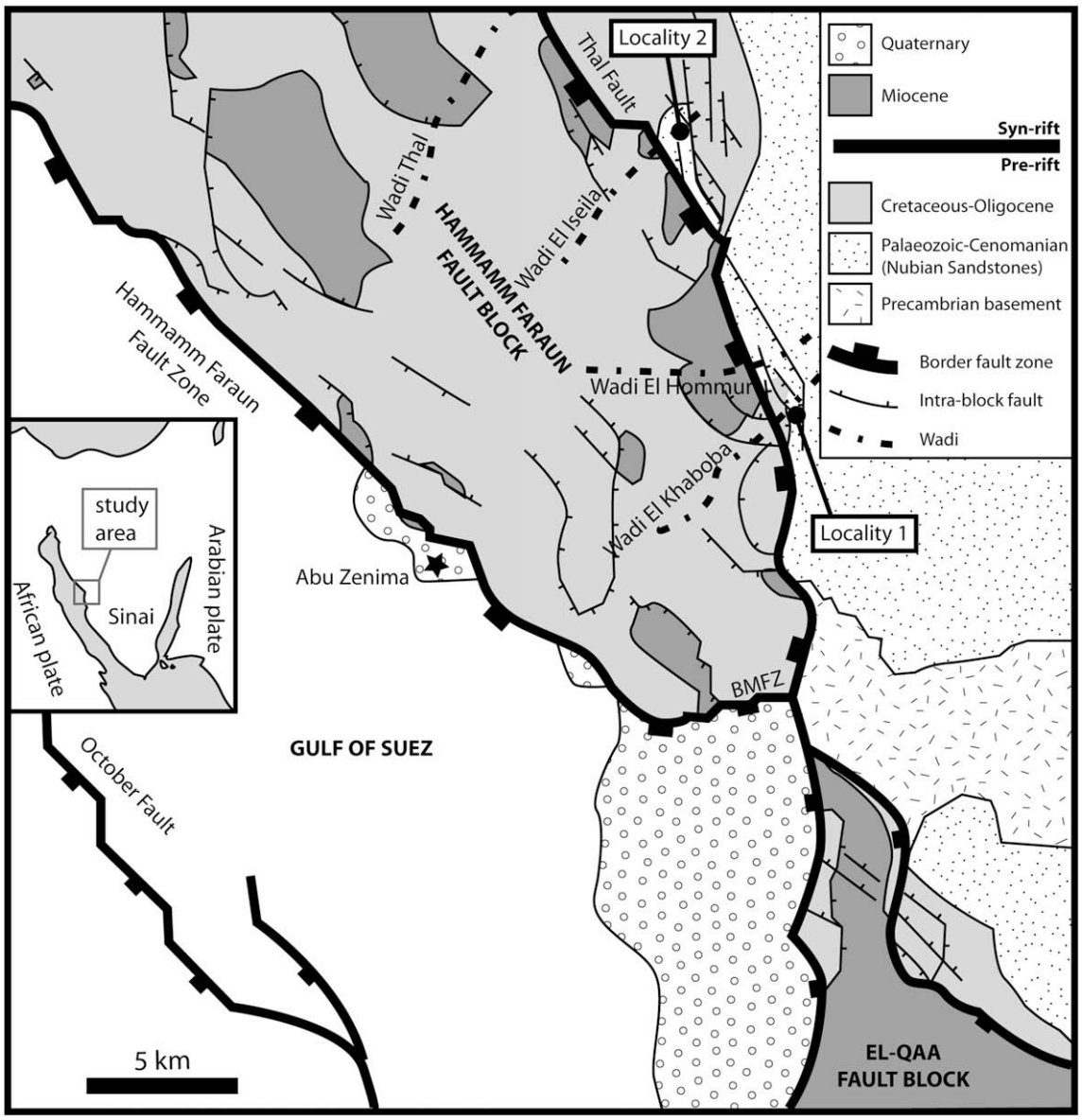

Fig. 1. Structural map of the Hammam Faraun Fault block and surrounding areas. The localities of the current study are indicated. Based on Moustafa (1993), Sharp et al. (2000) and Jackson et al. (2006).

Fossen et al., 2007) and good sorting and rounding, which produce high stress concentrations at grain contact points (Gallagher et al., 1974). In simple terms, cataclasis is regarded as a common deformation mechanism in porous sandstones having undergone faulting at depths greater than 1 km (e.g. Fisher and Knipe, 2001). In this work we focus on cataclastic deformation bands that differ from those described in the literature. Thus, in order to comprehend the differences appearing from the descriptions below, we first take a look at what we in the current study refer to as classical cataclastic deformation bands.

1.1. Classical cataclastic deformation bands

What is now considered the classical work on cataclastic deformation bands was carried out in the Entrada and Navajo Sandstones of southern Utah by Aydin (1978). Microstructurally, Aydin described the cataclastic deformation bands as 0.5 mm thick zones of grain crushing encapsulated in a zone of compaction and grain reorganization. Aydin and Johnson (1978) also presented a three-stage model for faulting in porous sandstones: (1) nucleation and growth of an individual deformation band, (2) formation of multiple deformation bands (cluster zones) due to strain hardening, and (3) the breakthrough of a continuous slip surface in the cluster zone. It is important to notice that slip surfaces in these rocks only occur after the accumulation of 10s or 100s of bands in a decimetre to metre thick zone. The findings of Aydin (1978) and Aydin and Johnson (1978) have later been supported by a number of field based studies, both from the same rock units (Antonellini and Aydin, 1995; Fossen and Hesthammer, 1998; Davis, 1999; Davatzes and Aydin, 2003; Shipton and Cowie, 2003; Johansen and Fossen, in press), and from similar rock units in the western USA (Jamison and Stearns, 1982; Sternlof et al., 2004), Great Britain (Underhill and Woodcock, 1987; Edwards et al., 1993; Beach et al., 1997), France (Wibberley et al., 2000, 2007), the North Sea (Hesthammer and Fossen, 2001) and numerous other places. Furthermore, experimental work gives additional support to their model (e.g. Mair et al., 2000; Lothe et al., 2002).

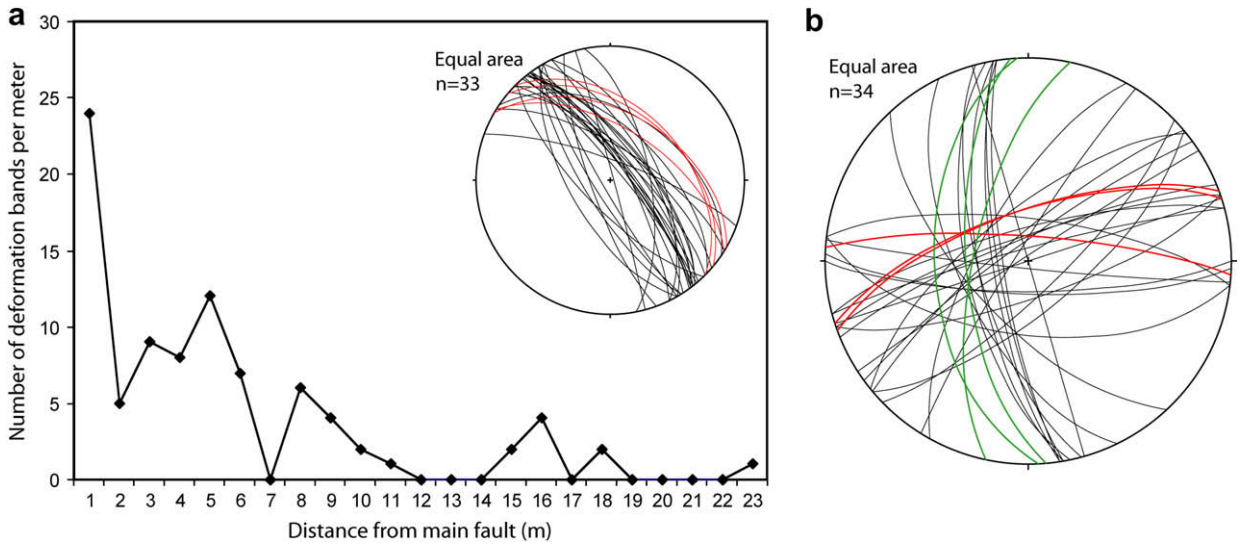

Fig. 2. (A) Damage zone profile from locality 1 in Wadi el Khaboba. The structure frequency profile records the number of deformation bands per metre against distance from main fault. The equal area stereo net shows that the bands (black great circles) strike sub-parallel to the main fault (red great circles) and thus are related to its formation. (B) Equal area stereo net showing the orientation of deformation bands and faults at locality 2 in Wadi El Iseila. The largest fault in the area is plotted as red great circles. The smaller but, for the studied outcrop, closer and more influential fault is plotted as green great circles. Black great circles represent deformation bands.

Previous work has established that deformation bands can alter the effective permeability of highly porous sandstones (e.g. Sternlof et al., 2004). For cataclastic deformation bands of the type studied by Aydin (1978), Aydin and Johnson (1978, 1983), Antonellini et al. (1994), the permeability measured across a single deformation band can be reduced by several orders of magnitude relative to that of an adjacent undeformed sample, with the greatest reductions occurring in the most permeable sandstones. Some of the published data (e.g. Antonellini and Aydin, 1994; Fisher and Knipe, 2001) indicate permeability contrasts of up to 6 orders of magnitude, while others report lower values (Taylor and Pollard, 2000). One reason for the locally high contrast reported by some authors is that permeability has been measured across multiple deformation bands, and a distinction between single and multiple bands is generally not made in published data sets. According to our own field data from localities in Utah (Fossen, unpublished), most single cataclastic deformation bands exhibit permeabilities 0–3 orders of magnitude lower than the adjacent host rock. The permeability reduction is due to the significant changes in porosity, pore-throat geometry and pore connectivity caused by grain crushing and reorganization.

The current study is based on outcrops of faulted pre-rift sandstones in the eastern flank of the late Oligocene to early Miocene Suez rift, in the Western Sinai Peninsula, Egypt (Fig. 1). In this area we identified and investigated cataclastic deformation bands that seem different from the classical bands described by Aydin (1978) and others. In particular, they do not comply with Aydin and Johnson's (1978) model, where a cluster of deformation bands is formed before the formation of a slip plane. Instead, the deformation bands described in this paper develop internal central slip planes within far-apart individual deformation bands that are unrelated to deformation band cluster zones. This study undertakes an investigation of these deformation bands, and seeks to:

1. document and describe their geometry and structural characteristics;
2. measure and assess their petrophysical properties and potential effect on fluid flow;
3. discuss how these deformation bands may have formed, and why they deviate from the classical model for fault initiation in porous sandstones.

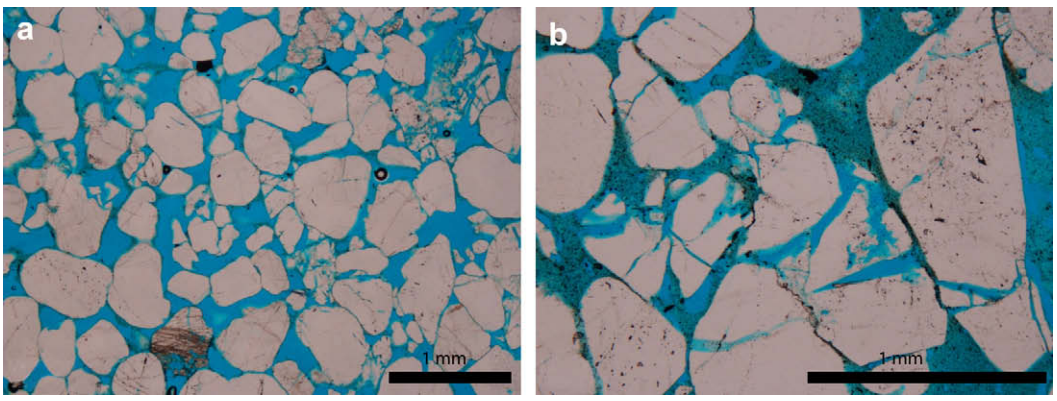

Fig. 3. Photomicrographs of host rock samples. Note that grain fracturing is abundant. The samples were treated with epoxy prior during thin section preparation, which makes the pore space stand out in blue colour.

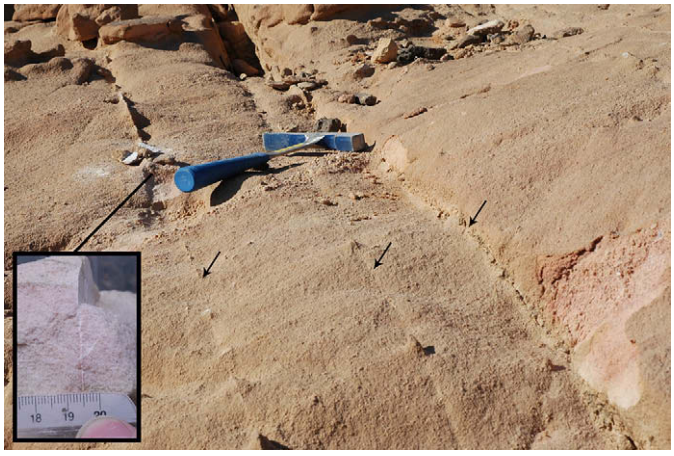

Fig. 4. Picture from the studied outcrop at locality 1 showing three individual deformation bands (indicated by arrows), all of which feature central slip planes. The inset shows a hand specimen taken from one of the deformation bands, where the slip plane is clearly visible. The scale bare on the inset is in centimetres.

2. Geological setting

The Suez rift is an aborted arm of the Red Sea rift system, forming a NW–SE trending basin, c. 300 km long and c. 80 km wide, separating the Sinai micro-plate from the African plate (Fig. 1A, e.g. Garfunkel and Bartov, 1977; Lyberis, 1988; Bosworth et al., 2005). The main phase of rifting occurred during the separation of the African and Arabian plates from the latest Oligocene until its termination in the Miocene (c. 24–15.5 Ma). Termination of rifting relates to initiation of the Dead Sea–Aqaba transform, which accommodates continued extension in the Red Sea rift (Cochran, 1983). The Suez rift is characterized by classical rift geometries featuring half-grabens and rotated normal fault blocks (e.g. Moustafa, 1993; Jackson et al., 2006). The current work is based on outcrop studies along extensional faults in the eastern shoulder of the Suez rift, c. 1.5 km into the footwall of the rift-bounding Thal Fault (Fig. 1), as described by Sharp et al. (2000). Deformation bands in the Nubian Sandstone of the hanging wall and footwall of these faults are the focus of this study. The term *Nubian Sandstone* (Shukri, 1945) refers to a regionally extensive succession of Cambrian to Early Cretaceous Sandstones in the NE African region (e.g. Bosworth, 1995). In Sinai, the Nubian Sandstone comprises predominantly non-marine fluvial sands, with a few marginal marine and aeolian interbeds (e.g. Gupta et al., 1999). At the localities featured in this study they are mainly fluvial. The maximum burial depth of the stratigraphic level of the study area at the time of faulting is about 1.5 km (Du Bernard et al., 2002).

3. Field data and results

3.1. Localities and field methods

We focus on two localities, at which a large number of deformation bands were examined. Both localities are found NE of the Hammam Faraun Fault block, along extensional faults that probably formed coevally with the larger Thal Fault. At both localities, the Nubian Sandstone comprises the hanging wall and footwall of the extensional faults.

At locality 1 (Wadi El Khaboba; Fig. 1) a NW striking fault displays an offset of c. 15 m; the sense of slip is normal, with a small sinistral strike-slip component. The fault core is characterized by a 5–15 cm thick zone of cataclasites derived from sandstones in the hanging wall and footwall, encapsulated by a 30–100 cm thick zone with a very high density of anastomosing cataclastic deformation bands. Several discrete slip planes in the core accommodate the majority of fault displacement. The studied deformation bands are found in the damage zone (Fig. 2A) of this fault, c. 1–30 m away from the fault core.

At locality 2 (Wadi El Iseila; Fig. 1), there are two faults affecting the Nubian Sandstone (Fig. 2B). The largest fault strikes WSW and has an offset of c. 150 m. The studied outcrop is 150–200 m into the footwall of this fault. There is also another smaller, but, for the studied outcrop, more influential fault, striking S with an offset of c. 15 m. This fault features a c. 1.2 m thick core comprising a c. 30 cm thick cataclasite, and a c. 90 cm thick zone of anastomosing deformation bands, displaying ladder and fishnet geometries (Davis, 1999; Schultz and Balasko, 2003). As on the previous locality, several discrete slip surfaces in the fault core have accommodated most of the fault displacement. The studied deformation bands are located 5–30 m into the hanging wall of the latter fault.

Numerous deformation bands were identified and recorded in the damage zones of the main faults, the results of which are outlined below. As the two localities are structurally very similar and both feature the same host rock unit, we treat the deformation band data recorded at the localities as *one* sample population in the following. Basic field methods were applied: compass, measuring tape and GPS were used to record orientations, offsets, thicknesses, spatial relationships and positioning. Furthermore, a mini-permeameter was used to collect permeability data, and samples for thin sections and laboratory analysis of petrophysical properties were collected.

3.2. Host rock

The host rock at both localities is fluvial sandstone from the Jurassic to Early Cretaceous Malha Formation (Abdallah and El Adindani, 1963) of the Nubian Sandstone succession. Grain sizes vary from medium to very coarse sand, and the stratigraphic units feature well preserved cross-stratification. The host rock is very loose, which may partly be a result of weathering, but largely a result of poor consolidation. The latter is common for sandstones at shallow burial depths, which may be relatively loose and friable at burial depths down to 2.5–3 km (Bjørlykke and Egeberg, 1993). Thin sections confirm only minor effects of burial diagenesis (Fig. 3A). Dissolution has occurred at some grain contacts but is not abundant. Cementation is practically non-existent, consistent with the shallow ($\sim$1.5 km) burial depths that the Nubian Sandstone has experienced in this area; quartz cementation occurs mainly at temperatures in excess of 90 °C (Walderhaug, 1996) or at depths in excess of 3.5 km (Bjørlykke and Høeg, 1997). Grain fracturing, however, is widespread in the host rock (Fig. 3B), particularly in coarse-grained sandstone layers. The degree to which grains are affected by fracturing varies from single fractures to complete grain breakdown. Grain fracturing is laterally relatively uniform within layers of similar grain size and is not constrained to rock volumes affected by faulting, but is in some thin sections seen to increase in intensity near the deformation bands.

3.3. Deformation bands in the field

The deformation bands observed in the current study (referred to as Sinai bands in the following) display characteristics that are both similar and different from classical cataclastic deformation bands (CCDB). The bands are recognized as cataclastic deformation bands based on three criteria: (1) displacement is detectable and on a mm- to cm-scale; (2) displacement is accommodated in a mm-thick, white coloured shear zone; (3) in the thin zone of shearing, grain size reduction is detectable by eye or hand lens, and further

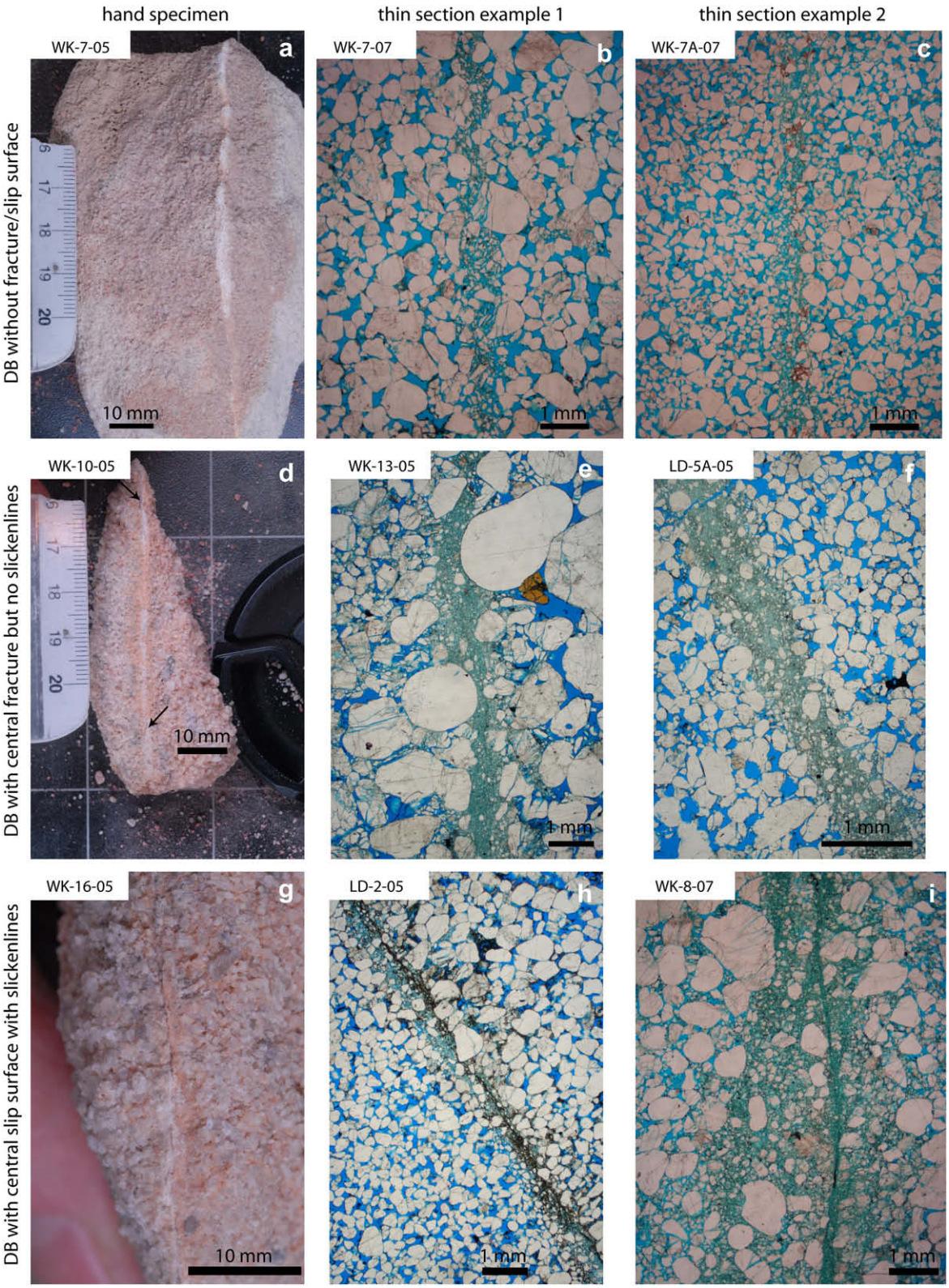

Fig. 5. Field photos and photomicrographs of deformation band samples collected in the field. (A–C) Deformation bands without fracture/slip surface. (D–F) Deformation bands with a central fracture but no slickenlines. (G–I) Deformation bands with a central slip surface with slickenlines.

confirmed by thin section analysis and SEM images (see below). Although these criteria match those of CCDB, the Sinai deformation bands display other characteristics that are not compatible with CCDB. Most notably, many of the deformation bands feature slip planes within widely spaced individual bands that are not associated with deformation band clusters (Fig. 4). The fractures/slip planes are subtle features that appear as inherent parts of the deformation bands. Deformation bands without slip surfaces were also identified, and the following visual subdivision was made in the field: (1) deformation bands with no visible fracture or slip

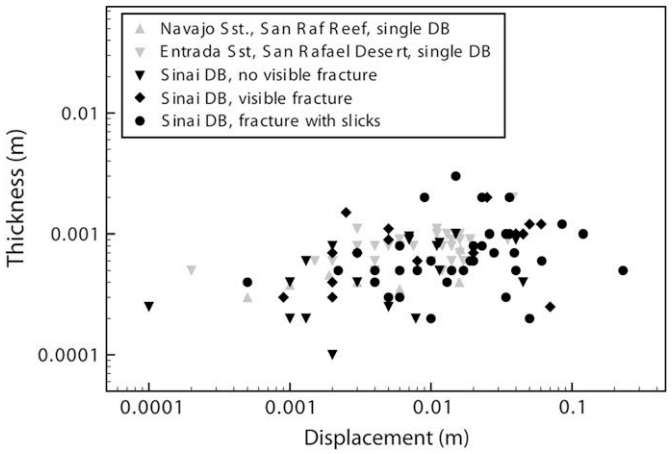

Fig. 6. Log–log plot of displacement vs. thickness of deformation bands. Three series of field measurements from Sinai are plotted: Deformation bands with no fracture plane, deformation bands with a central fracture but no slickenlines, and deformation bands with a central slip plane with slickenlines. In addition, two series from Utah (unpublished) are plotted, from the Navajo Sandstone and the Entrada Sandstone, respectively.

Table 1
Mean offset and mean thickness of deformation bands

Deformation band population	*n*	Mean offset (mm)	Mean thickness (mm)
Def. bands without central fracture	27	7.9	0.6
Def. bands with central fracture but no slickenlines	16	21.3	0.9
Def. bands with central slip surface with slickenlines	39	29.9	0.8
Total	82	21.0	0.8

Only bands were both offset and thickness were successfully recorded are included.
n = number of measurements.

plane (Fig. 5A); (2) deformation bands with a visible central fracture (Fig. 5D); (3) deformation bands featuring a central fracture with visible slickenlines (Fig. 5G). Fractures/slip surfaces occur exclusively within deformation bands and fracture occurrence outside of deformation bands is negligible. Thus, the orientations of the fractures/slip planes follow those of the deformation bands that they sit within and correspond with the orientation of the main faults at the two localities (Fig. 2A and B). Deformation bands and their inherent fractures/slip surfaces feature orientations that are both synthetic and antithetic relative to the main fault. Inspection of the slickenlines seen on slip surfaces within single deformation bands indicates that the slip is of the same sense as that of the main faults at the respective localities (e.g. close to normal slip to the NE for synthetic and to the SW for antithetic bands/slip surfaces at locality 1, see Fig. 2A). The fracture planes and slip planes seen in some of the deformation bands were of varying continuity, ranging from patchy cm-scale occurrences to completely continuous along much of the strike of the deformation band (Fig. 5D and G). Thus, the three subdivisions described above are commonly found at various places along the length of a single deformation band.

3.4. Offset and thickness

The studied deformation bands feature thicknesses similar to or slightly less than CCDB (Fig. 6), the mean thickness of the bands being 0.8 mm (Table 1). Offsets are larger than those known for CCDB, the maximum offset recorded being 230 mm and the mean offset being 21 mm (Table 1). There is no strong correlation between offset and thickness, which is typical for cataclastic deformation bands. The thickness of the Sinai bands remains stably at around 0.8 mm for most bands, regardless of the amount of offset. However, the Sinai data indicate a correlation between the amount of offset and the development and growth of a central slip surface. Where the offset is less than c. 15 mm there is a mix of bands with no slip plane, bands with fracture planes but no slickenlines and bands with slip planes featuring slickenlines. Where offset exceeds c. 15 mm, however, practically all bands feature slip planes with slickenlines (Fig. 6). It thus appears that beyond this value, displacement is no longer accommodated by cataclastic shear, but rather accommodated by slip along a discrete slip surface.

3.5. Cataclasis and grain size distribution

The cataclastic cores of the bands in the current study exhibit grain crushing ranging from mild grain breakdown to extremely intense cataclasis (Fig. 5). The most intense grain crushing is observed in bands containing a central fracture or slip surface (Fig. 7A). This is supported by statistical analysis of particle size distribution obtained from Backscattered Electron Images (BSE) using image processing methods (Torabi et al., 2007).

The results are presented graphically in Fig. 8, where plots of log EF vs. log particle size areas (PSA) have been investigated.

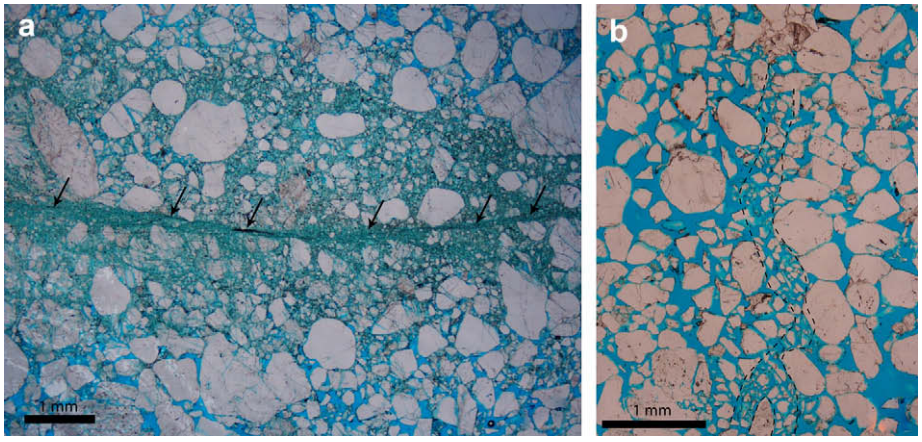

Fig. 7. (A) Thin section of slipped deformation band showing severe crushing near the slip surface, indicated by arrows. (B) Photomicrograph of incipient deformation band. Incipient deformation bands represent the earliest stage of development for the studied deformation bands.

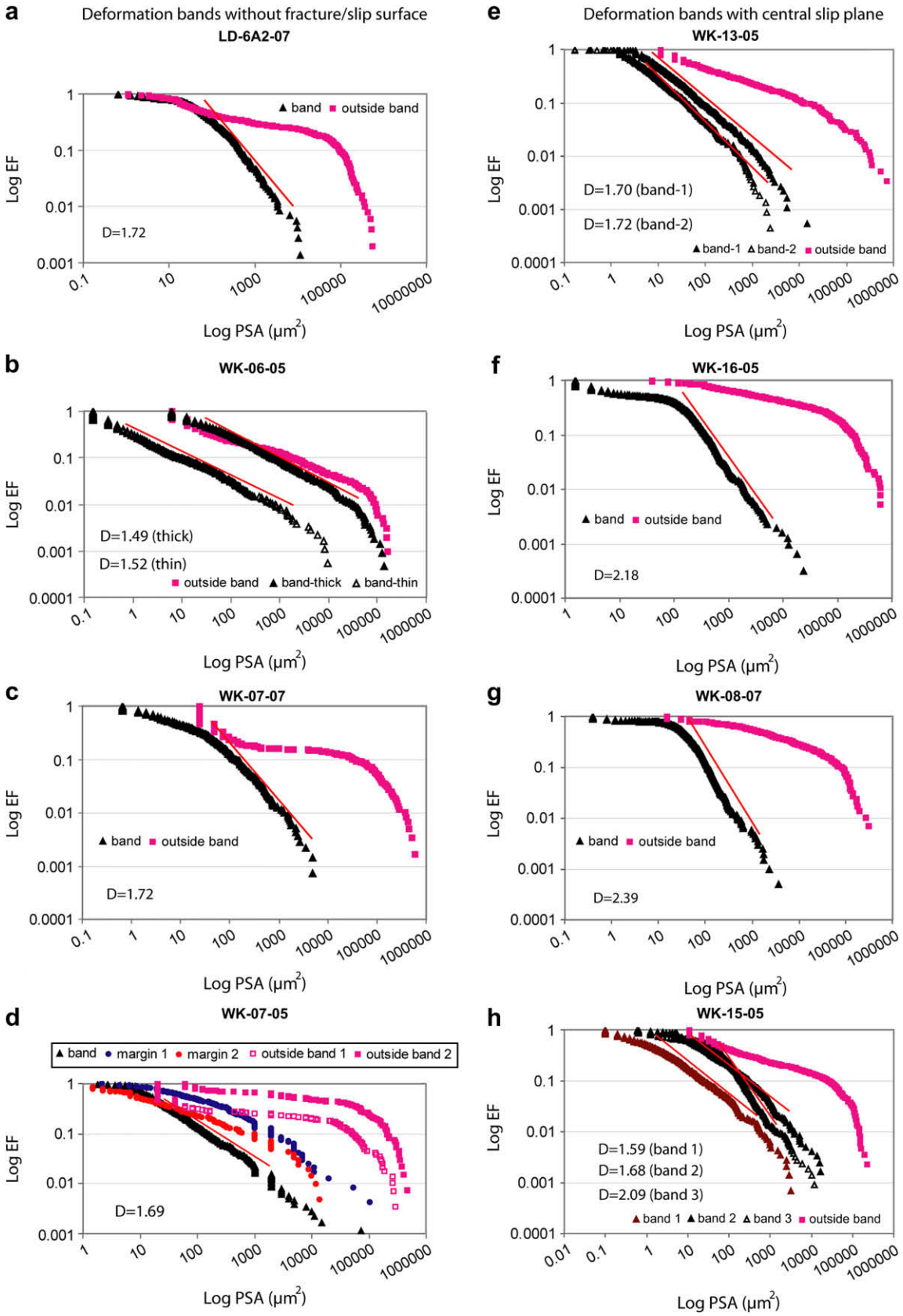

Fig. 8. Results from statistical analysis of particle size distribution obtained from Backscattered Electron Images (BSE). Log EF (Exceedence Frequency) is plotted against log PSA (particle size area). (A–D) Deformation bands with no visible fracture. (E–H) Deformation bands with a central fracture. All of these, except (E), feature visible slickenlines.

Table 2
Deformation band particle size distribution data

Sample no.	*n*	*D*	R^2	Slip surface
LD-6A2-07	732	1.72	0.9824	No
WK-06-05 thick band	2183	1.49	0.9715	No
WK-06-05 thin band	1815	1.52	0.9896	No
WK-07-07	1400	1.72	0.9734	No
WK-07-05	1715	1.69	0.9668	No
WK-13-05 band1	1867	1.7	0.9954	Fracture, no SL
WK-13-05 band2	2258	1.72	0.9927	Fracture, no SL
WK-16-05	3164	2.18	0.9696	Yes
WK-08-07	2048	2.39	0.9772	Yes
WK-15-05 band1	1450	1.59	0.9926	Uncertain
WK-15-05 band2	1217	1.68	0.981	Uncertain
WK-15-05 band3	2172	2.09	0.9864	Yes

Note that for some thin sections, multiple bands were analysed.
n Denotes the number of data points (measured grains) for each sample. *D* is the 3D power law dimension (or simply *D*-value).
R^2 is the coefficient of determination, indicating the power law fit to the particle size distribution (where 0 is no fit and 1 is a perfect fit).

Exceedence Frequency (EF) of a particular value of a measured variable is defined as the number of data with values greater than that value, divided by the total number of the data. In each of the examined thin sections, images of the host rock outside of the band as well as the band itself have been investigated. The particle size distribution plots show that, for all of the analysed samples, there is a reduction of grain size in the bands relative to the host rock. The host rocks have a majority of grain sizes at c. 0.1–1 mm^2, as indicated by a change in slope around 0.1 mm^2. The kinked or curved appearance of most host rock particle size distribution plots is different from the straight lines or curves with straight central segments seen in the deformation band particle size distribution plots. This is typical of cataclastically deformed sand (e.g. Sammis et al., 1987). In these cases the particle size distribution of the bands can be described by a power law with dimension *D* (exponent). The calculated two-dimensional *D* can be converted to the third dimension by adding 1 (Sammis et al., 1987; Blenkinsop, 1991; Torabi et al., 2007). The value of the three-dimensional *D* is presented in Table 2.

Particle size distribution plots from the margin of the deformation bands show distributions intermediate between those of the host rock and the band (Fig. 8D and H). In general, there is a positive correlation between the value of *D* and the intensity of cataclasis: high *D*-values indicate strong cataclasis. The bands hosting a central slip plane feature the highest *D*-values (2.09–2.39) and thus have undergone the most intense cataclasis (Table 2). Nevertheless, there are still some unbroken large grains in many of the bands (Fig. 5H). The intensity of the cataclasis is lower in the bands without a central slip surface ($D = 1.49$–1.72) than in those containing slip surfaces (Figs. 6 and 9, Table 2). Bands with the least intense cataclasis, i.e. where the grain breakdown is mild and limited, appear to have undergone much less deformation and are thus labelled *incipient bands* (Fig. 7B). These are bands that do not host a central fracture or slip surface. The relationship between these incipient bands and more mature bands will be addressed further in Section 5.

3.6. Architecture

The core of classical cataclastic deformation bands is known to be encapsulated in a zone of compaction and grain reorganization (Aydin, 1978). However, the bands in the current study feature no such zone of compaction (Fig. 9). Instead the bands display a sharp transition between undeformed host rock and the cataclastic core. The transition is sharpest across bands that contain a central slip plane, as the cataclasis is most intense here.

The slip surfaces themselves are easy to identify as discontinuities within the cataclastic core of the band (Fig. 5I). Most slip surfaces do not appear as open fractures in thin section. However, precipitated black minerals (probably iron oxides and/or hydroxides, Fig. 10) provide evidence for palaeo-fluid flow and precipitation along the slip surfaces.

4. Petrophysical properties

4.1. Methods

Porosity and permeability measurements have been carried out using different field, laboratory and image analysis techniques. For

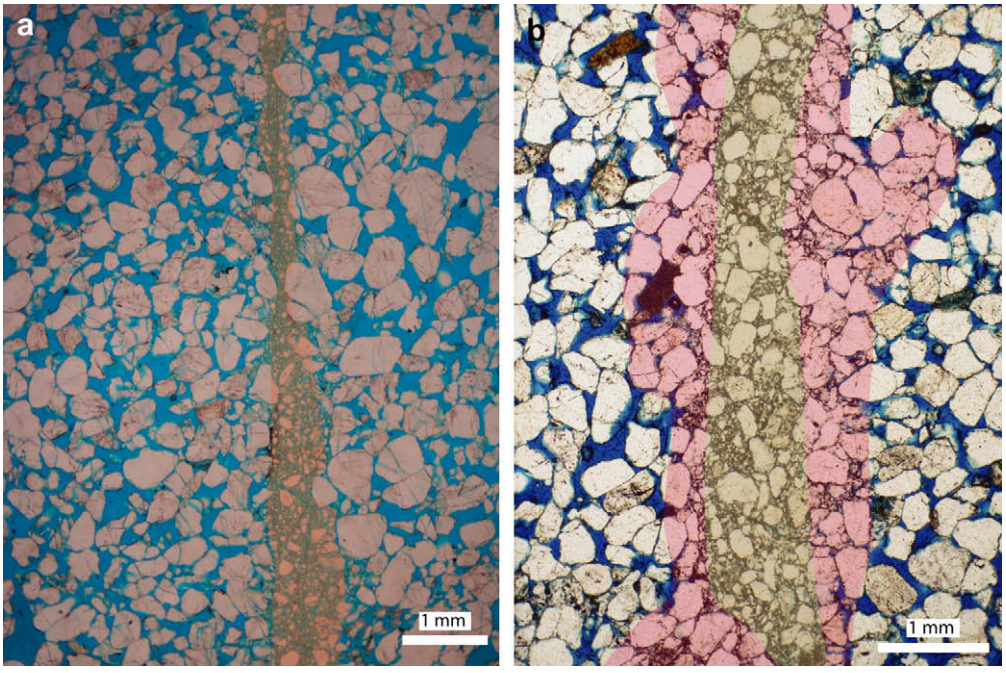

Fig. 9. (A) Photomicrograph showing typical deformation band architecture of the bands in the current study. Note that there is a cataclastic core, but no surrounding compactional envelope. (B) Architecture of a classical cataclastic deformation band with a cataclastic core and a zone of compaction enveloping the core. This photomicrograph is from the Navajo Sandstone in Utah and is modified from Fossen and Gabrielsen (2005).

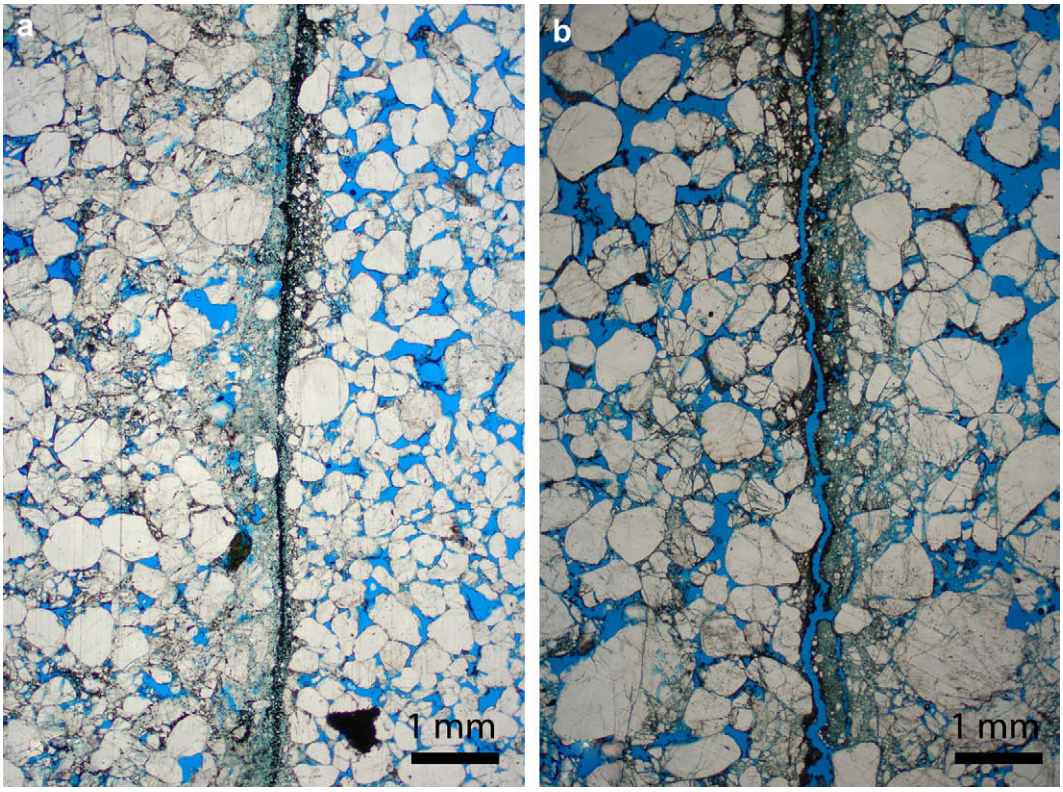

Fig. 10. Photomicrographs of deformation bands hosting a central slip surface with slickenlines. Note the black precipitated minerals (probably ferric oxides) in the centre of the bands, which we interpret as evidence for palaeo-fluid flow along the slip surfaces.

porosity, image analysis techniques using optical microscopy for host rock samples and SEM imagery for deformation band samples were applied (for a description of this method see Torabi et al., in press). A total of 44 porosity determinations using this technique were conducted on a selection of thin sections from collected hand samples. Eleven of these were host rock thin sections and 33 thin sections with deformation bands. In addition to this, one sample was analysed at ResLab Reservoir Laboratories in Stavanger, Norway, where helium porosity by Boyle's law technique was determined.

For permeability, a combination of mini-permeameter field measurements and laboratory experiments was applied. The laboratory measurements were conducted at ResLab Reservoir Laboratories, determining the Klinkenberg-corrected gas permeability (Klinkenberg, 1941) by the steady state technique. Eight core plugs, drilled and sampled in the field, were analysed using this method. Of these, two were host rock samples, two were samples with single bands with slip surface and four were samples taken from slip surfaces along the main fault in locality 1. In addition to this, measurements were conducted in the field using a TinyPerm II Portable Air Permeameter (mini-permeameter) manufactured by New England Research (see Appendix A). Permeabilities from 43 sample locations in the field were determined using this method. Of these were eight host rocks, 10 bands with no slip surface, five bands with fracture plane but no visible slickenlines, and 20 bands hosting a slip surface with slickenlines.

4.2. Porosity

The results from the porosity determinations are shown in Fig. 11A. The data are organized by type of sample: host rock, incipient bands, bands without slip surface and bands with a central slip surface.

The data show that host rock porosity and porosity of incipient bands fall within approximately the same range of values (21–35% for host rock samples and 24–35% for incipient bands). This is in agreement with observations from thin sections (Fig. 7B), which show that porosity is relatively unchanged in such bands. However, the populations of deformation bands *without* and *with* slip surfaces fall within a relatively lower range of porosity values (10–26% and 9–32%, respectively), although there is overlap with host rock and incipient band porosities. The large variations of porosity values within the deformation bands are probably explained by differences in amount and localization of cataclasis in the bands. For one of the samples, a porosity profile across a deformation band (featuring a central slip surface) was made (Fig. 11B). The profile shows a porosity drop across a band from the host rock, via the margin to the centre of the cataclastic core. However, porosity in the bands is surprisingly high (lowest value being 9%) when compared with other studies of cataclastic deformation bands (Fig. 11A). The implications of this are addressed in Section 5.

4.3. Permeability

Permeability results from laboratory and mini-permeameter measurements are shown in Fig. 12A. The results are separated according to sample type: host rock, bands with no visible fracture, bands with a visible central fracture but no slickenlines, and, finally, bands hosting a central slip surface with slickenlines. In addition, a population of laboratory measurements from main fault slip surfaces at locality 1 is shown. Incipient bands have not been tested for permeability due to difficulties excavating a surface suitable for mini-permeameter measurements. Furthermore, samples of incipient bands for laboratory determination of permeability were too loose to be fit for analysis. All measurements represent

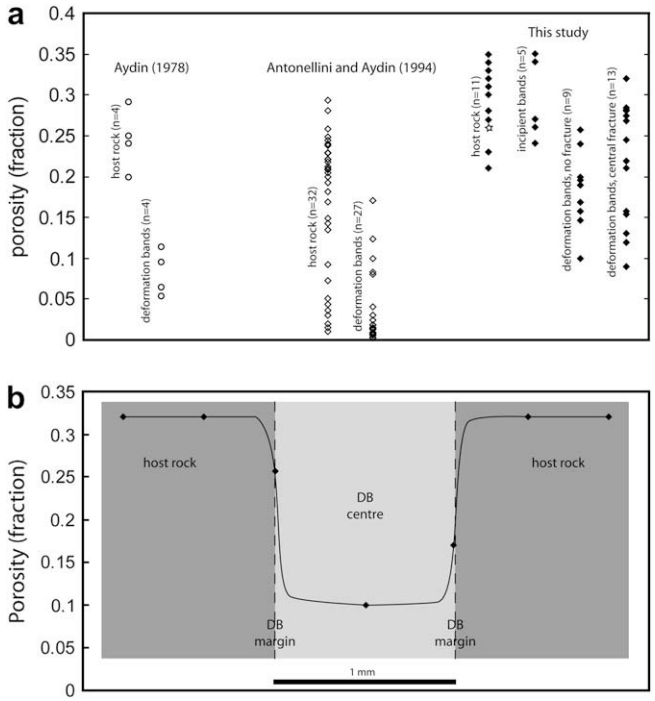

Fig. 11. (A) Porosity data for deformation bands of the current study compared to data from Aydin (1978) and Antonellini and Aydin (1994). The samples from the current study were analysed using image analysis techniques, except for one for which the porosity was determined in the laboratory (see text for details). The open star denotes the laboratory sample. (B) Porosity profile across a single cataclastic deformation band. The geometry of the extrapolation curve between data points is inferred from thin section studies, which indicate abrupt transitions in grain size from host rock to deformation band.

permeability of flow *across* the band. Band-parallel permeability was not measured.

The permeametry data reveal a distinctly reduced permeability in all bands relative to the host rock. The host rock permeability values range from 4000 to 53,000 mD with a mean of 13,000 mD. These values are extremely high and probably inaccurate due to the mini-permeameter's limitations in resolving permeabilities above 10,000 mD. However, note that the laboratory measurements fall within the range of the mini-permeameter measurements. We therefore consider the measured values to be sufficiently accurate for comparative purposes. The different types of bands feature permeability values 1.5–4.5 orders of magnitude lower than those of the host rock. Deformation bands without any fracture or slip surface display permeability values between 13.7 and 64.3 mD, with a mean of 31.1 mD. The bands with a central fracture but no slickenlines fall within the range of 4.0–26.2 mD, with a mean of 14.6 mD. Finally, the bands hosting a central slip plane with slickenlines display permeabilities of 1.7–22.1 mD, with a mean of 7 mD. Hence, there is an increase in permeability contrast (relative to the host rock) from bands with no fracture development (1.5–3.5 orders of magnitude), via bands with a central fracture but no slickenlines (2–4 orders of magnitude), to bands with a central slip surface with slickenlines (up to 4.5 orders of magnitude). A permeability reduction of 1.5–4.5 orders of magnitude is within the high range of our own and previously published data for deformation band permeability (see Fig. 12B and e.g. Antonellini and Aydin, 1994; Ahlgren, 2001; Fisher and Knipe, 2001; Lothe et al., 2002). Mini-permeameter measurements of slip planes in the core of the main fault at locality 1 record a lower permeability reduction of approximately 1.5–2.5 orders of magnitude.

5. Discussion

The deformation bands examined in this work occur in highly porous sandstones and are visually very similar to classical cataclastic deformation bands (CCDB). Furthermore, grain comminution is an important deformation mechanism at the microscale, and none of the bands accumulate large (metre-scale) displacement. However, detailed investigation reveals differences that are significant (Table 3). The Sinai bands deviate from CCDB in several aspects. Firstly, they lack a grain compaction envelope around the cataclastic zone and, secondly, they exhibit more pronounced cataclasis. However, the most outstanding difference occurs when a central fracture forms in the bands, which localizes most of the subsequent strain accumulation to a zone that is narrower than the original band. At this point, the life of the deformation band as such is over, and it is converted into a *slipped deformation band*. The ensuing discrete slip explains why Sinai bands have accumulated more offset (we have recorded offsets up to 230 mm) than CCDB, which become inactive after accumulating 3–4 cm offset at the most.

The development history of the deformation bands described in the current study can be inferred from the interpretation of different developmental stages, based on the thin sections. The least developed and most pristine bands are the so-called incipient bands (Fig. 7B), in which cataclasis is mild and no porosity reduction has taken place (Fig. 11A). Bands with higher offsets show pronounced cataclasis but no fracture plane/slip surface (Fig. 5A–C), and, finally, the highest offsets are exhibited by bands with a central fracture or slip surface (Fig. 5D–I). We believe that these represent increasingly progressed stages of the evolution of the Sinai bands, and the following model for the evolution of the deformation bands is suggested (see Fig. 13):

1. Scattered grain crushing due to vertical loading (compaction) (Fig. 13A).
2. Nucleation of a cataclastic deformation band (Fig. 13B). Mild cataclasis, no porosity reduction (incipient band).
3. Progressive shear and cataclasis. The band now displays pronounced cataclasis (Fig. 13C). Porosity is mildly reduced but still relatively high.
4. Progressive shear, cataclasis and nucleation of a fracture plane in the centre of the band. The fracture nucleates in patches along the band (Fig. 5D), which gradually propagate and coalesce until the fracture is continuous along the entirety of the band (Fig. 5G). No significant further reduction of porosity.
5. Discrete slip on the fracture plane. Slickenlines form. Extreme cataclasis develops near the slip surface (Figs. 7A and 13D). No significant further reduction of porosity.

The reactivation of Sinai bands and the resulting formation of a central slip surface contradict the widely accepted concept of strain hardening within CCDB (Aydin, 1978), where a zone of deformation bands form prior to the formation of a slip surface. There is no obvious reason why a similar pattern is not seen in the Sinai bands, and a fair question to ask is whether the major mechanics of deformation must change drastically from one step to the next in the above evolution: do the different elements above represent different events (deformation episodes), with different stress configurations and different principal stress directions? In isolation, the apparent different modes of failure seen in the morphology of the slipped deformation bands in Sinai may suggest so. However, a consideration of all the field evidence indicates otherwise. Considering the spatial arrangement of deformation bands it is clear that they correspond well with the main faults at the respective localities, and therefore arguably were formed in conjunction with one another, under the same overall stress

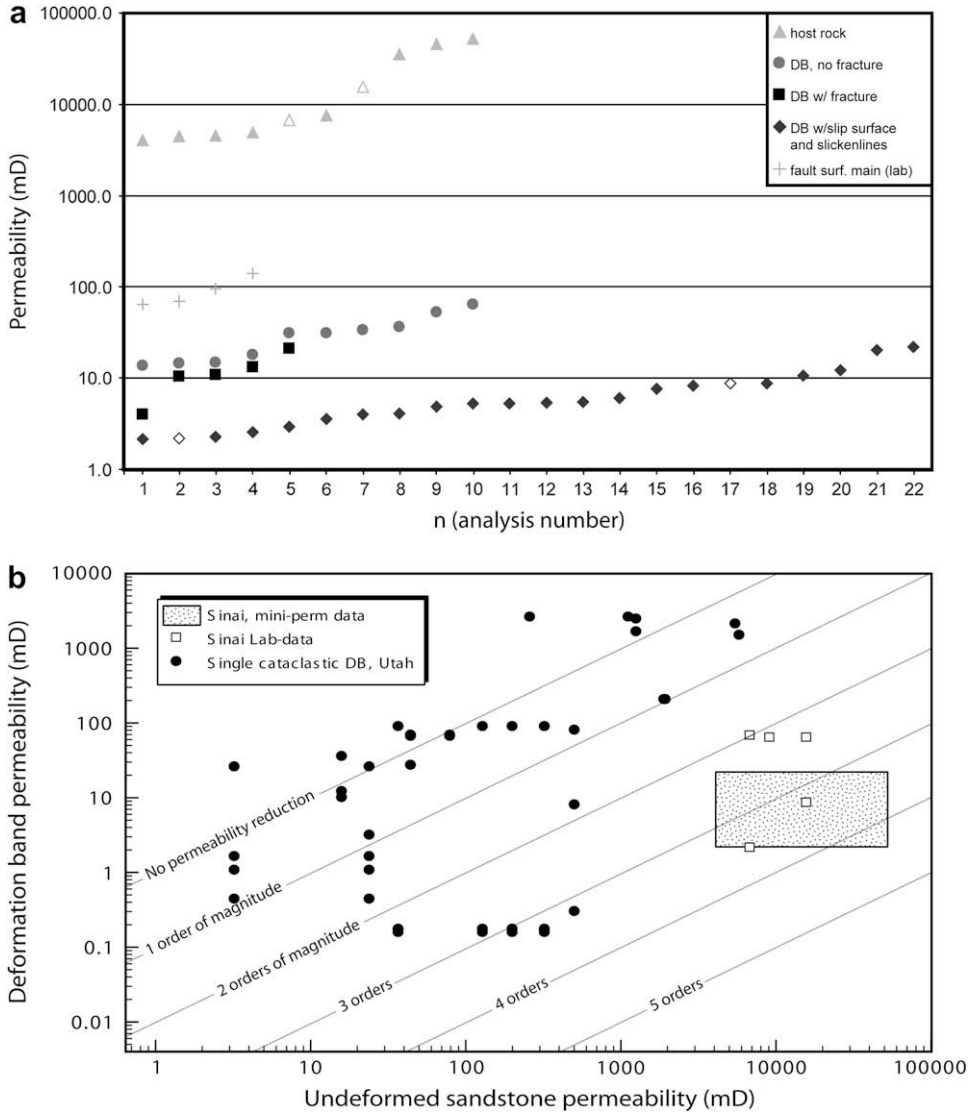

Fig. 12. (A) Deformation band permeability data. Open data points indicate laboratory measurements of permeability, whereas the filled points are mini-permeameter measurements (see text for details). (B) Permeability contrast data from the current study (bands with central slip surface) plotted together with our own data from single deformation bands (CCDB) in Utah (unpublished).

regime. Furthermore, the fractures/slip surfaces found at the localities occur exclusively within deformation bands and thus follow the same orientation trend as the bands and main faults. Also, the slickenlines observed on slip surfaces within individual deformation bands correspond well with those of the main faults. This indicates that the stress field during the formation of deformation bands and discrete slip planes occurred under the same general stress field. If the fractures/slip planes had formed under a different stress configuration than the cataclastic shear bands, we would also expect to see fractures occurring outside of the

Table 3
Comparative properties of classical cataclastic deformation bands and the Sinai bands

Criteria	Classical bands	Sinai bands
Similarities		
Appearance in outcrop	White streaks	White streaks
Thickness	Very thin, mostly ~1 mm	Very thin, mostly ≤1 mm
Displacement	mm- to cm-scale displacement	mm- to cm-scale displacement
Thickness–displacement correlation	Weak correlation	Weak correlation
Differences		
Architecture	Compaction zone enveloping cataclastic core	No compaction zone enveloping core
Accommodation of shear displacement	Grain reorganization and cataclasis	Cataclasis and discrete slip
Strain distribution	Strain distributed across core and compaction zone	Very localized strain
Geomechanical response to failure	Strain hardening	Strain softening
Response to post-nucleation additional stress	New band formation	Reactivation and slip plane formation
Shear mode	Compactional shear	Closer to simple shear
Porosity inside band	Very low – some times as low as 1% or less	Relatively high, 9–32%
Permeability contrast	0–3 Orders of magnitude (our single band measurements)	1.5–4.5 Orders of magnitude

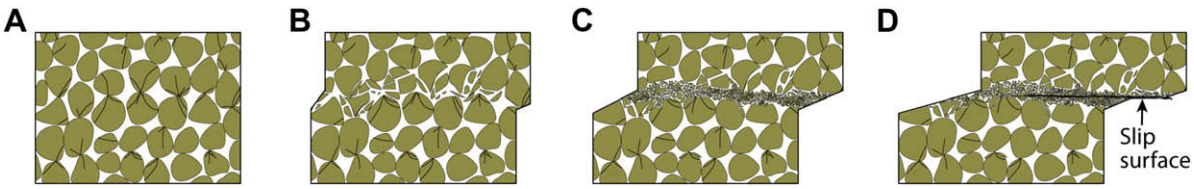

Fig. 13. Schematic of the proposed evolutionary stages of slipped deformation bands: (A) scattered grain crushing due to vertical loading; (B) incipient band featuring mild cataclasis; (C) progressive shear causes increasingly intense cataclasis; (D) a central fracture develops along which discrete slip eventually takes place. See text for details.

deformation bands, and with different orientations than the deformation bands. This is clearly not the case here. These structures thus contrast previous accounts of deformation bands and associated (sheared) joints (Zhao and Johnson, 1992; Davatzes and Aydin, 2003), where the different types of structures are demonstrably related to completely separable events in the regional geological history of the areas in question.

An alternative model is offered by unloading during rift flank uplift and denudation. As the rocks are brought to shallower levels, unloading is an inevitable result. This could lead to opening of fractures and subsequent discrete slip. However, given progressive uplift and unloading it is likely that the remote and local stress configuration would change, and it is difficult to envision the axes of principal stress retaining their orientation through extended periods of uplift. As argued earlier, a change in the overall stress configuration is not supported by our observations.

The question thus remains, why a central slip plane is generated rather than multiple adjacent bands, as seen in Utah and many other places. Clues may perhaps be found in the abundant grain fracturing of the host rock and/or the relatively high porosity observed in the Sinai bands compared to that of CCDB (Fig. 11A, Antonellini and Aydin, 1994). The proposed mechanical evolution for the deformation bands described in the current study can be illustrated in a *Q*–*P* diagram (Fig. 14), where the mean and differential stresses are plotted along the horizontal and vertical axes, respectively. In this diagram the yield envelope (e.g. Antonellini et al., 1994; Borja and Aydin, 2004; Wong et al., 2004; Wibberley et al., 2007), which depends on grain size, porosity and other rock properties, separates elastic from permanent (inelastic) strain. Dilation occurs in the left part of the envelope (at low mean stress), simple shear in the top part (at high differential stress) and pure compaction where the yield cap intersects the horizontal axis (at relatively high confining pressure). Pure compaction thus occurs at or near zero differential stress at what is referred to as the grain crushing pressure P^* (Zhang et al., 1990). The widespread grain fracturing seen in the Nubian Sandstone, also where it is unaffected by faulting, indicates that the state of stress in the sandstone at some point was close to P^*. This abundant grain fracturing must have been caused by the weight of the overburden. We suggest that the local grain crushing pressure (P^*1 in Fig. 14) was reached prior to deformation band formation, probably at the time of maximum burial. There are two lines of evidence supporting this view. Firstly, the grain fractures in the host rock are not constrained to rock volumes affected by faulting and are therefore arguably not related to the faulting itself. Secondly, the maximum burial of these rocks (c. 1.5 km, Du Bernard et al., 2002) was probably reached before or at the time of rift initiation. After rift initiation, the rocks did not undergo further burial, but rather embarked on a course of uplift and denudation, which is common in rift flank settings (Chery et al., 1992). The time of the already shallow maximum burial depth is perceived as the only time around which pervasive grain fracturing would likely occur (see below), and the grain fracturing must therefore arguably predate the faulting and resulting deformation bands.

Although not a common feature for sandstones at shallow burial depths, experimental work has demonstrated that such fracturing may occur at low stresses (2–6 MPa, Chuhan et al., 2002). Interestingly, experiments in the same study have also shown that microfractures can form during compaction that are not visible under the microscope. Such fractures cause a general weakening of the sandstone that promotes cataclasis. Yet, pervasive grain fracturing is more common at higher stress levels, which at shallow depths could be promoted by low pore pressure (Wong and Baud, 1999; Baud et al., 2000). Furthermore, the large host rock grain sizes are more prone to grain fracturing than their fine-grained equivalents at low stresses (lower than 5 MPa, Chuhan et al., 2002).

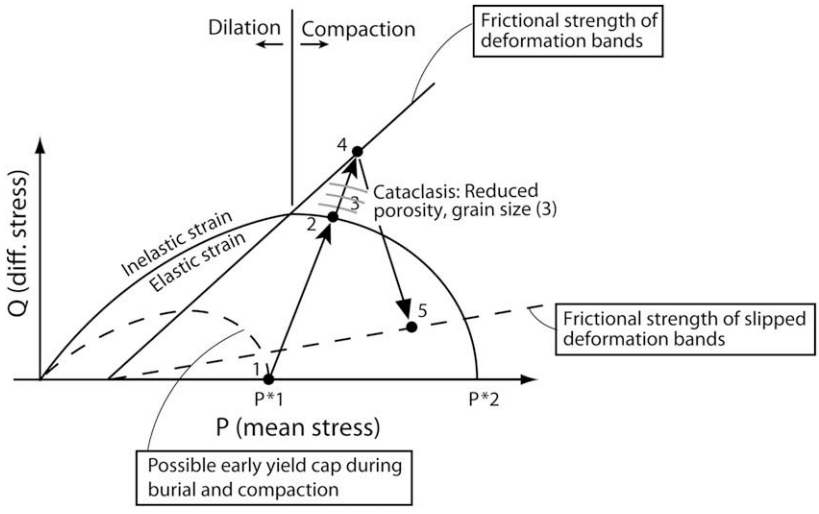

Fig. 14. *Q*–*P* diagram (differential stress vs. mean stress) applied to porous rocks (modified from Fossen et al., 2007). Numbers 1–5 indicate the stages of development for deformation bands investigated in this study, see text for details. The yield surface/cap will 'inflate' if grain size and porosity are reduced, as indicated by grey lines at stage 3.

A combination of these effects may thus have been at work to achieve the level of background grain fracturing seen in the host rock.

We speculate that abundant pre-existing grain fractures in the host rock may promote cataclasis as differential stress builds up and deformation bands form (stage 2 above and in Fig. 14). The grain fractures represent micro-discontinuities that weaken the rock locally, and therefore represent locations where deformation bands can nucleate and grow, especially if the microfractures are orientated favourably relative to the applied stress. As cataclasis is a process of grain fracturing, a cataclastic deformation band is essentially a compilation of microfractures. In CCDB, stress concentration at the contact point of unfractured grains is allowed to build up until eventually causing failure. Although this is clearly also the case for the bands in Sinai, we believe that the background fracturing of the host rock grains may have had two important effects that make these bands different: (1) the grains fail earlier and without a preceding phase of shear-induced compaction; (2) upon failure, inter-granular fractures grow faster and may have a preferred orientation as fracture growth may follow preferentially oriented intragranular grain fractures. Thus, shear-induced cataclasis (stages 2–3 above and in Fig. 14) may progress faster and be more severe than for a CCDB under the same applied stress. Furthermore, if inter-granular fractures attain a preferred orientation parallel to the band, they may strongly contribute to local weakening within the band. Hence, the band becomes susceptible to brittle failure and forms a through-going slip surface (stages 4–5 above and in Fig. 14).

Evidence for the high-intensity cataclasis is found in the particle size distribution data and the magnitude of the three-dimensional power law dimension D. As previously mentioned, the high values of D (2.09–2.39, Table 2) recorded in the bands with slip planes indicate that the cataclasis is severe. If compared to particle size distribution plots from CCDB in the damage zone of the Bartlett Fault, SE Utah (Fig. 15, $D = \sim 1.4$–1.5), the value of the three-dimensional D is evidently much higher in the Sinai bands containing slip surfaces than in the Utah bands. Thus, the cataclasis is significantly less severe in CCDB from the Bartlett Fault than that of the slipped deformation bands in the current study. However, for Sinai bands *without* a central fracture/slip surface, the D-values (1.49–1.72) are comparable, although slightly higher, to those from the Bartlett Fault.

Porosity is another factor that may have an effect. Higher porosity affects the yield cap envelope and may lower the critical pressure required for failure (Fig. 14, Schultz and Siddharthan, 2005; Fossen et al., 2007). Hence, the high porosity within the bands may cause the Sinai bands to be more susceptible to subsequent brittle failure than CCDB. The CCDB, undergoing much more syn-kinematic compaction to the point of complete destruction of porosity, will increase the required critical pressure for subsequent failure (reactivation) and thus strain harden. As the Sinai bands preserve porosity to a larger degree, they have not strain hardened to any significant extent. Thus, the combined effect of preserved porosity and the presence of intragranular fractures in the host rock make the Sinai bands represent zones of weakness after initial failure.

The difference in porosity between the Sinai bands and CCDB furthermore suggests that dissimilar modes of deformation are involved in their formation. Whereas CCDB form during compactional shear (resulting in very low porosity), the relatively high porosity in the Sinai bands indicates that they were formed by a mode closer to simple shear. This also explains why there is no compaction zone enveloping the cataclastic zone.

The permeability data presented in this paper are, as previously mentioned, in the upper range of our own and previously published petrophysical data for CCDB (Fig. 12B). There are systematic variations, however, with a gradual increase in permeability contrast (relative to matrix permeability) from bands with no slip plane through to bands with fully developed slip surfaces. Permeability contrast also increases with the severity of the cataclasis affecting the same bands. The progressive cataclasis and the associated destruction of pore connectivity explain the stepwise increase of the permeability contrast described above. Additionally, slip surface wall rocks make efficient sealing membranes, bringing the permeability contrast to a maximum where they are present.

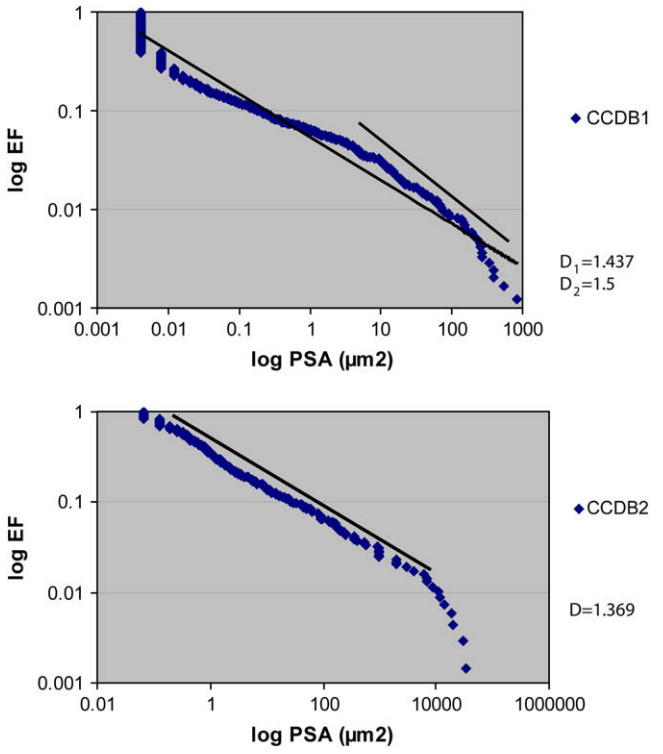

Fig. 15. Particle size distribution data from two deformation bands in the damage zone of the Bartlett Fault, Utah (unpublished). Note that for deformation band CCDB1, two values of the power law dimension D have been calculated, one for the entirety of the data series (D_1), and one for the steepest segment (D_2).

The recorded permeability data have implications for fluid flow. Should such deformation bands occur in a subsurface reservoir, they would represent potential baffles to flow, even more so than CCDB. What is not captured by our permeability measurements, however, is the effect of intra-band slip surfaces on flow *parallel* to the band. The formation of slip surfaces within the bands may give rise to significantly anisotropic permeability, in that the slip surfaces may represent fractures along which fluids can flow. Because of this, their impact on reservoir performance is likely to be significantly different to that of CCDB. Whereas CCDB generally reduce permeability and are considered negative in a reservoir setting, bands with slip planes, although baffles to band-normal flow, represent potential conduits for band-parallel flow. Depending on the continuity and interconnectedness of such bands, they might actually have a positive effect on reservoir communication.

6. Summary and conclusions

A new type of cataclastic deformation bands has been presented, and a model for their evolution suggested. Based on the collected data and field observations, we draw the following conclusions:

1. The cataclastic deformation bands described in this work are different from classical cataclastic deformation bands

described in the existing literature (e.g. Aydin, 1978). The Sinai bands are characterized by intense cataclasis, relatively little compaction, strain weakening and, in many cases, discrete slip along a central slip surface. The bands are thought to have formed under near simple shear conditions.

2. The background grain fracturing observed in the host rock, combined with the limited porosity collapse, is the most probable explanation for the deviation from the classical model for faulting in porous clastic rocks (Aydin and Johnson, 1978).
3. The deformation bands feature porosities that are significantly higher than published figures for cataclastic deformation bands elsewhere (e.g. Antonellini and Aydin, 1994).
4. Permeability data fall in the high range of data for classical cataclastic deformation bands, particularly where slip surfaces are developed (Fig. 12B and e.g. Antonellini and Aydin, 1994; Lothe et al., 2002).
5. In a reservoir setting, the structures may represent baffles to cross-band flow, but slip surfaces also represent fractures *along* which fluids may flow. The bands may therefore act as conduits to band-parallel flow and increase connectivity within a hydrocarbon or groundwater reservoir.

Acknowledgements

Ian Sharp is thanked for directing us to the outcrops used in this study. Eivind Bastesen is thanked for assistance and discussions in the field. Nestor Cardozo is thanked for critical reviews of the manuscript. The authors wish to acknowledge the Fault Facies project for funding this study through the financial project support granted by the Norwegian Research Council, StatoilHydro and ConocoPhillips. Reviewers A. Aydin and C. Wibberley are thanked for their useful comments, which greatly improved this manuscript.

Appendix A. Mini-permeameter analysis procedure

Measurements were conducted using a TinyPerm II Portable Air Permeameter (mini-permeameter) manufactured by New England Research. When recording permeability data, the operator pressures a rubber nozzle against the specimen and withdraws air from it with a single stroke of a syringe. As air is pulled from the sample, a micro-controller unit simultaneously monitors the syringe volume and the transient vacuum pulse created at the sample surface. Using signal processing algorithms the micro-controller computes the response function of the sample/instrument system. The response function is related to permeability K:

$$T = -0.8206 \log_{10}(K) + 12.8737,$$

where T is the value of the response function and the recorded output from the mini-permeameter. When performing the tests in the field, the deformation bands were excavated, carefully removing part of the hanging wall of the deformation band. Once access was gained to the surface of the band/slip surface, the tests were performed as described above. For each sample point 3–5 measurements were made, in order to ensure the quality of the data. For each sample point, an average of the measurements was calculated and used as the representative value for that point.

References

Abdallah, A.M., El Adindani, A., 1963. Stratigraphy of upper Paleozoic rocks, western side of the Gulf of Suez. In: Geological Survey of Egypt Paper, No. 25, 18 pp.
Ahlgren, S.G., 2001. Exploring the formation, microtexture, and petrophysical properties of deformation bands in porous sandstone. AAPG Bulletin 85, 2046.
Antonellini, M., Aydin, A., 1994. Effect of faulting on fluid flow in porous sandstones: petrophysical properties. AAPG Bulletin 78, 355–377.
Antonellini, M., Aydin, A., 1995. Effect of faulting on fluid flow in porous sandstones: geometry and spatial distribution. AAPG Bulletin 79, 642–671.
Antonellini, M., Aydin, A., Pollard, D.D., 1994. Microstructure of deformation bands in porous sandstones at Arches National Park, Utah. Journal of Structural Geology 16, 941–959.
Aydin, A., 1978. Small faults formed as deformation bands in sandstone. Pure and Applied Geophysics 116, 913–930.
Aydin, A., Johnson, A.M., 1978. Development of faults as zones of deformation bands and as slip surfaces in sandstone. Pure and Applied Geophysics 116, 931–942.
Aydin, A., Johnson, A.M., 1983. Analysis of faulting in porous sandstones. Journal of Structural Geology 5, 19–31.
Baud, P., Zhu, W., Wong, T.-F., 2000. Failure mode and weakening effect of water on sandstone. Journal of Geophysical Research 105, 16371–16389.
Beach, A., Brown, J.L., Welbon, A.W., McCallum, J.E., Brockbank, P.J., Knott, S.D., 1997. Characteristics of fault zones in sandstones from NW England: application to fault transmissibility. In: Meadows, N.S., Trueblood, S.P., Hardman, M., Cowan, G. (Eds.), Petroleum Geology of the Irish Sea and Adjacent Areas. Geological Society, London, Special Publications, vol. 124, pp. 315–324.
Bense, V.F., Van den Berg, E.H., Van Balen, R.T., 2003. Deformation mechanisms and hydraulic properties of fault zones in unconsolidated sediments; the Roer Valley Rift System, The Netherlands. Hydrogeology Journal 11, 319–332.
Bjørlykke, K., Egeberg, P.K., 1993. Quartz cementation in sedimentary basins. AAPG Bulletin 77, 1538–1548.
Bjørlykke, K., Høeg, K., 1997. Effects of burial diagenesis on stresses, compaction and fluid flow in sedimentary basins. Marine and Petroleum Geology 14, 267–276.
Blenkinsop, T.G., 1991. Cataclasis and processes of particle size reduction. Pure and Applied Geophysics 136, 59–86.
Borja, R.I., Aydin, A., 2004. Computational modeling of deformation bands in granular media. I. Geological and mathematical framework. Computer Methods in Applied Mechanics and Engineering 193, 2667–2698.
Bosworth, W., 1995. A high-strain rift model for the southern Gulf of Suez (Egypt). In: Lambiase, J.J. (Ed.), Hydrocarbon Habitat in Rift Basins. Geological Society, London, Special Publications, vol. 80, pp. 75–102.
Bosworth, W., Huchon, P., McClay, K., 2005. The Red Sea and Gulf of Aden Basins. Journal of African Earth Sciences 43, 334–378.
Chery, J., Lucazeau, F., Daignieres, M., Vilotte, J.P., 1992. Large uplift of rift flanks: a genetic link with lithospheric rigidity? Earth and Planetary Science Letters 112, 195–211.
Chuhan, F.A., Kjeldstad, A., Bjørlykke, K., Høeg, K., 2002. Porosity loss in sand by grain crushing – experimental evidence and relevance to reservoir quality. Marine and Petroleum Geology 19, 39–53.
Cochran, J.R., 1983. A model for development of the Red Sea. AAPG Bulletin 67, 41–69.
Davatzes, N.C., Aydin, A., 2003. Overprinting faulting mechanisms in high porosity sandstones of SE Utah. Journal of Structural Geology 25, 1795–1813.
Davis, G.H., 1999. Structural Geology of the Colorado Plateau Region of Southern Utah, with Special Emphasis on Deformation Bands. The Geological Society of America, 157 pp.
Du Bernard, X., Labaume, P., Darcel, C., Davy, P., Bour, O., 2002. Cataclastic slip band distribution in normal fault damage zones, Nubian sandstones, Suez rift. Journal of Geophysical Research 107, doi:10.1029/2001JB000493.
Edwards, H.E., Becker, A.D., Howell, J.A., 1993. Compartmentalization of an aeolian sandstone by structural heterogeneities: permo-Triassic Hopeman Sandstone, Moray Firth, Scotland. In: North, C.P., Prosser, D.J. (Eds.), Characterization of Fluvial and Aeolian Reservoirs. Geological Society, London, Special Publications, vol. 73, pp. 339–366.
Fisher, Q.J., Knipe, R.J., 2001. The permeability of faults within siliciclastic petroleum reservoirs of the North Sea and Norwegian Continental Shelf. Marine and Petroleum Geology 18, 1063–1081.
Fossen, H., Gabrielsen, R.H., 2005. Strukturgeologi. (Structural Geology Textbook). Fagbokforlaget, Bergen, 375 pp. (in Norwegian).
Fossen, H., Hesthammer, J., 1997. Geometric analysis and scaling relations of deformation bands in porous sandstone. Journal of Structural Geology 19, 1479–1493.
Fossen, H., Hesthammer, J., 1998. Deformation bands and their significance in porous sandstone reservoirs. First Break 16, 21–25.
Fossen, H., Schultz, R.A., Shipton, Z.K., Mair, K., 2007. Deformation bands in sandstone – a review. Journal of the Geological Society (London) 164, 755–769.
Gallagher, J.J., Friedman, M., Handin, J., Sowers, G.M., 1974. Experimental studies relating to microfracture in sandstone. Tectonophysics 21, 203–247.
Garfunkel, Z., Bartov, Y., 1977. Tectonics of the Suez rift. Geological Survey of Israel Bulletin 71, 1–41.
Gupta, S., Underhill, J.R., Sharp, I.R., Gawthorpe, R.L., 1999. Role of fault interactions in controlling synrift sediment dispersal patterns: Miocene, Abu Alaqa Group, Suez rift, Sinai, Egypt. Basin Research 11, 167–189.
Hesthammer, J., Fossen, H., 2001. Structural core analysis from the Gullfaks area, northern North Sea. Marine and Petroleum Geology 18, 411–439.
Jackson, C.A.L., Gawthorpe, R.L., Leppard, C.W., Sharp, I.R., 2006. Rift-initiation development of normal fault blocks: insights from the Hammam Faraun fault block, Suez rift, Egypt. Journal of the Geological Society (London) 163, 165–183.
Jamison, W.R., Stearns, D.W., 1982. Tectonic deformation of Wingate Sandstone, Colorado National Monument. AAPG Bulletin 66, 2584–2608.
Johansen, T.E.S., Fossen, H., 2008. Internal deformation of fault damage zones in interbedded siliciclastic rocks. In: Geological Society, London, Special Publications, 299, pp. 35–56.

Klinkenberg, L.J., 1941. The permeability of porous media to liquid and gases. In: Drilling and Production Practice. American Petroleum Institute, pp. 200–213.
Knipe, R.J., Fisher, Q.J., Jones, G., Clennell, M.R., Farmer, A.B., Harrison, A., Kidd, B., McAllister, E., Porter, J.R., White, E.A., 1997. Fault seal analysis: successful methodologies, applications and future directions. In: Møller-Pedersen, P., Koestler, A.G. (Eds.), Hydrocarbon Seals: Importance for Exploration and Production. Norwegian Petroleum Society, Special Publication, vol. 7, pp. 15–40.
Lothe, A.E., Gabrielsen, R.H., Bjørnevoll-Hagen, N., Larsen, B.T., 2002. An experimental study of the texture of deformation bands; effects on the porosity and permeability of sandstones. Petroleum Geoscience 8, 195–207.
Lyberis, N., 1988. Tectonic evolution of the Gulf of Suez and the Gulf of Aqaba. Tectonophysics 153, 209–220.
Mair, K., Main, I., Elphick, S., 2000. Sequential growth of deformation bands in the laboratory. Journal of Structural Geology 22, 25–42.
Mandl, G., DeJong, L.N.J., Maltha, A., 1977. Shear zones in granular material. Rock Mechanics 9, 95–144.
Moustafa, A.R., 1993. Structural characteristics and tectonic evolution of the east-margin blocks of the Suez rift. Tectonophysics 223, 281–299.
Sammis, C., King, G., Biegel, R., 1987. The kinematics of gouge deformation. Pure and Applied Geophysics 125, 777–812.
Schultz, R.A., Balasko, C.M., 2003. Growth of deformation bands into echelon and ladder geometries. Geophysical Research Letters 30, 2033, doi:10.1029/2002GL018449.
Schultz, R.A., Siddharthan, R., 2005. A general framework for the occurrence and faulting of deformation bands in porous granular rocks. Tectonophysics 411, 1–18.
Sharp, I.R., Gawthorpe, R.L., Armstrong, B., Underhill, J.R., 2000. Propagation history and passive rotation of mesoscale normal faults: implications for syn-rift stratigraphic development. Basin Research 12, 285–306.
Shipton, Z.K., Cowie, P.A., 2003. A conceptual model for the origin of fault damage zone structures in high-porosity sandstone. Journal of Structural Geology 25, 333–345.
Shipton, Z.K., Evans, J.P., Robeson, K.R., Forster, C.B., Snelgrove, S., 2002. Structural heterogeneity and permeability in faulted aeolian sandstone: implication for subsurface modeling of faults. AAPG Bulletin 86, 863–883.
Shukri, N.M., 1945. Geology of the Nubian sandstone. Nature 156, 116.
Sternlof, K.R., Chapin, J.R., Pollard, D.D., Durlofsky, L.J., 2004. Permeability effects of deformation band arrays in sandstone. AAPG Bulletin 88, 1315–1329.
Taylor, W.L., Pollard, D.D., 2000. Estimation of in-situ permeability of deformation bands in porous sandstone, Valley of Fire, Nevada. Water Resources Research 36, 2595–2606.
Torabi, A., Braathen, A., Cuisiat, F., Fossen, H., 2007. Shear zones in porous sand: insights from ring-shear experiments and naturally deformed sandstones. Tectonophysics 437, 37–50.
Torabi, A., Fossen, H., Alaei, B., 2008. Application of spatial correlation functions in permeability estimation of deformation bands in porous rocks. Journal of Geophysical Research 113, B08208, doi:10.1029/2007JB005455.
Underhill, J.R., Woodcock, N.H., 1987. Faulting mechanisms in high porosity sandstones; New Red Sandstone, Arran, Scotland. In: Jones, M.E., Preston, R.M.F. (Eds.), Deformation of Sediments and Sedimentary Rocks. Geological Society, London, Special Publications, vol. 29, pp. 91–105.
Walderhaug, O., 1996. Kinetic modeling of quartz cementation and porosity loss in deeply buried sandstone reservoirs. AAPG Bulletin 80, 731–745.
Wibberley, C.A.J., Petit, J.-P., Rives, T., 2000. Mechanics of cataclastic 'deformation band' faulting in high-porosity sandstone, Provence. Comptes Rendus de l'Académie des Sciences 331, 419–425.
Wibberley, C.A.J., Petit, J.-P., Rives, T., 2007. The mechanics of fault distribution and localization in high-porosity sands, Provence, France. In: Couples, G.D., Lewis, H. (Eds.), The Relationship between Damage and Localization. Geological Society, London, Special Publications, vol. 289, pp. 19–46.
Wong, T.-F., Baud, P., 1999. Mechanical compaction of porous sandstones. Oil & Gas Science and Technology – Review IFP 54, 715–727.
Wong, T.-F., David, C., Menébdez, B., 2004. Mechanical compaction. In: Guéguen, Y., Boutéca, M. (Eds.), Mechanics of Fluid-saturated Rocks. Elsevier, Amsterdam, pp. 55–114.
Zhang, J., Wong, T.-F., Davis, D.M., 1990. Micromechanics of pressure-induced grain crushing in porous rocks. Journal of Geophysical Research 95, 341–352.
Zhao, G., Johnson, A.M., 1992. Sequence of deformations recorded in joints and faults, Arches National Park, Utah. Journal of Structural Geology 14, 225–236.